

# **An Examination of the Chromium-Rich Passive Film's Formation on Alloy 22 in Mildly Alkaline Environments**

Todd S. Mintz,<sup>1</sup> Hipolito J. Gonzalez,<sup>2</sup> and Yi-Ming Pan<sup>1</sup>

Center for Nuclear Waste Regulatory Analyses<sup>1</sup>  
Southwest Research Institute®  
6220 Culebra Road  
San Antonio, Texas 78238-5166  
(210) 522-5282  
tmintz@swri.org

U.S. Nuclear Regulatory Commission<sup>2</sup>  
Two White Flint North  
11545 Rockville Pike  
Washington, DC 20555

## **ABSTRACT**

The passivity of Alloy 22 is attributed to the presence of a chromium-rich oxide film. However, in some alkaline environments, such as simulated concentrated water, a chromium-rich passive film has not been observed. It is believed that the chromium-rich passive film should be present because of the measured low corrosion rates. A silica/carbon contamination layer noted on the surface of Alloy 22 could also contribute to the observed low corrosion rates. A thermodynamic analysis was conducted to analyze the formation of the chromium-rich passive film. Solution compositions examined by other investigators where chromium oxides were not detected have been evaluated with commercial software to develop potential-pH diagrams. The thermodynamic data indicate that a chromium-nickel oxide ( $\text{NiCr}_2\text{O}_4$ ) is thermodynamically stable and may be a likely contributor to the observed low corrosion rates. Failure to observe the film is probably due to it being masked by a thick outer layer on the surface in combination with the dimensions of the film.

## **INTRODUCTION**

The waste package design for the potential geologic repository for high-level radioactive waste at Yucca Mountain, Nevada, currently considered by the U.S. Department of Energy includes an outer container made of Alloy 22 (Ni-22Cr-13Mo-4Fe-3W) for corrosion resistance.<sup>1</sup> Ni-Cr-Mo alloys are highly corrosion resistant nickel-based alloys. The corrosion resistance of Alloy 22 has been attributed to the chromium-rich passive film formed on the surface of the alloy, which is stable over a wide range of environmental conditions, and the incorporation of high valence elements (e.g., Mo and W) into the passive film limiting the susceptibility to localized corrosion (crevice or pitting corrosion).

Passivity occurs when an alloy forms a very thin and protective film on its surface in aqueous solutions leading to a significant decrease in the general corrosion rate. Insoluble compounds that form on the surface of an alloy by precipitation are considered not to provide as much protection against corrosion. Passivity of Alloy 22 occurs in a range of electrochemical potentials, temperatures, and chemical environments. At high corrosion potentials, Alloy 22 will lose passivity and exhibit transpassive dissolution with corrosion rates one or two orders of

magnitude higher than under passive conditions.<sup>2</sup> Alloy 22 may lose passivity in aggressive environments (e.g., Mg-Cl solutions at elevated temperatures).<sup>2</sup> Chromium-containing alloys have been recognized as forming very stable and thin passive films. The structure and composition of passive films are in general difficult to determine because of the dimensions of these films (few nanometers thick). In many instances a bilayer structure can be discerned in passive films. The inner layer is made of a chromium-rich oxide that is considered to be responsible for passivity.<sup>3</sup> The outer layer in general forms by a dissolution and precipitation process. The outer layer may contribute to the overall corrosion rate of the alloy, but generally not to the same extent as the inner chromium-rich oxide.

Recent studies of Alloy 22 in various simulated repository solutions have attempted to characterize the passive film composition and thickness in alkaline conditions<sup>4,5</sup> using techniques such as x-ray photoelectron spectroscopy (XPS) with argon sputtering and electron energy loss spectroscopy (EELS). Examination of Alloy 22 oxide film grown in some mildly alkaline solutions (pH 8.6-10.2) suggested that in some instances there was no detectable chromium oxide.<sup>4,5</sup> The exact nature of the oxide could not be determined in these tests. However, it is believed that the thin chromium oxide existed at the metal interface because of the low corrosion rates measured in these environments.<sup>6,7</sup>

Although a chromium-rich oxide was not observed on Alloy 22 in the solutions considered by other investigators, as mentioned previously, a contamination layer was present on the oxide layer. The observed contamination layers were identified as either a silica (SiO<sub>2</sub>) or a carbon surface layer.<sup>4,5</sup> It was likely that silica contamination occurred because of dissolution from the glass test cell in basic solutions. Similarly, the carbon contamination layer may have resulted because of partial dissolution of tank linings. Both silica and carbon films have been used in the past as corrosion inhibitors<sup>8-14</sup> and may contribute to the low corrosion rates in these simulated repository environments.

Silica has been used to promote the formation of a corrosion protective layer for various material-environment combinations.<sup>8-11</sup> Amaral and Muller<sup>8</sup> examined the effect of silica on iron and showed that the silica increased the film resistance and reduced the corrosion rate. Silica has also been found to increase the resistance to pitting and general corrosion on 304 stainless steel.<sup>9</sup> Silica has been analyzed in the corrosion of nuclear steam generators.<sup>10,11</sup> Navas, et al.<sup>10</sup> examined the effect of various forms of silica on the corrosion resistance of Alloy 600. Results from these studies indicate that silica is a corrosion inhibitor.

Ensinger, et al. and Von Ringleben, et al. showed that an amorphous carbon film on aluminum can decrease the pitting corrosion susceptibility in aggressive solutions.<sup>12,13</sup> The effect of hydrogenated amorphous carbon films was examined on Ni-Ti alloys by Sui and Cai.<sup>14</sup> The results of this study indicated that the hydrogenated amorphous carbon films can improve the corrosion resistance of Ni-Ti alloys.

The objective of this review is to evaluate the potential formation of the chromium-rich passive film in mildly alkaline solutions where such a film was not observed. In particular, the solutions examined in this paper were originally evaluated experimentally by Chiang, et al.<sup>4</sup> to examine the stress corrosion cracking susceptibility of Alloy 22. Experimental tests were conducted to examine the stress corrosion cracking of Alloy 22 in various simulated Yucca Mountain groundwater chemistries. During the initial tests, anodic species that constitute these solutions were selectively removed. The stress corrosion cracking susceptibility decreased significantly

when bicarbonate was removed from the simulated solution. The next series of tests evaluated the effect of bicarbonate and chloride ions. In the solutions studied, the bicarbonate was the predominant constituent that was correlated to stress corrosion cracking susceptibility. The oxide film was evaluated by XPS in these environments, and under conditions where stress corrosion cracking was possible, the chromium concentration in the oxide film was significantly lower compared to the oxide formed in benign solutions. In some of the solutions examined, a chromium oxide film was not detectable. These solutions are the focus of this paper.

This study aims to investigate the possible presence of chromium-rich oxide in the passive film by evaluating the thermodynamic data for Alloy 22 in weakly alkaline solutions at 95 °C [203 °F]. In these simulated environments, the chromium-rich passive film is believed to be present because of low corrosion rates observed for Alloy 22. However, because of the contamination layer that may also contribute to the low corrosion rates, additional evidence is needed to establish the existence of a chromium-rich passive film. The thermodynamic analyses are compared to the XPS data on Alloy 22 by Chiang, et al.<sup>4</sup> in mildly alkaline environments. The comparison is used as an approach to understand the potential formation of a chromium-rich passive film on Alloy 22 in these solutions where a chromium oxide was not detected.

## METHODS

In this analysis, calculations were performed using Corrosion Analyzer™, Version 2.0 software developed by OLI Systems, Inc. (Morris Plains, New Jersey). The model used in Corrosion Analyzer is designed to provide a representation of chemical equilibria and thermophysical properties in the bulk solution and metal-solution interface thermodynamics. The fundamental aspects of the speciation and thermophysical model in the Corrosion Analyzer were described by Anderko and Lencka.<sup>15,16</sup> The stability diagram (potential-pH) model was described by Anderko, et al.<sup>17</sup>

The chemical composition to approximate Alloy 22 for the thermodynamic calculation is provided in Table 1. Because the chromium-rich oxide film was not observed in some of the mildly alkaline environments evaluated in the study by Chiang, et al.<sup>4</sup>, these particular solutions were examined. These simulated solutions are shown in Table 3 and include (a) 0.19 M NaCl + 1.14 M NaHCO<sub>3</sub>, (b) 1.14 M NaHCO<sub>3</sub>, and (c) simulated concentrated water (SCW), which is described in Table 2. In addition to these alkaline solutions, one neutral solution (0.19 M NaCl), where a chromium-rich oxide was observed at a higher potential (400 mV<sub>SCE</sub>), was also examined.

<b>Table 1. Chemical Composition (wt%) of Alloy 22</b>											
<b>Ni</b>	<b>Cr</b>	<b>Mo</b>	<b>W</b>	<b>Fe</b>	<b>Co</b>	<b>Si</b>	<b>Mn</b>	<b>V</b>	<b>P</b>	<b>S</b>	<b>C</b>
Balance	21 (21.4)*	13.5 (13.3)	0 (2.8)	6 (3.8)	0 (1.2)	0 (0)	0 (0.2)	0 (0.1)	0 (0)	0 (0)	0.02 (0)
Ni–nickel; Cr–chromium; Mo–molybdenum; W–tungsten; Fe–iron; Co–cobalt; Si–silicon; Mn–manganese; V–vanadium; P–phosphate; S–sulfur; C–carbon *From experimental tests <sup>1</sup>											

This solution, 0.19 M NaCl, was selected in order to examine the individual effect of chloride on the formation of the chromium-rich passive film. The pH of the three bicarbonate ( $\text{HCO}_3^-$ ) containing solutions, was adjusted to 9 at 25 °C [77 °F] by adding sodium hydroxide as titrant in the calculation, which was similarly done in the experimental tests.<sup>4</sup> The calculated pH and chemical species of the electrolyte solutions at 95 °C [203 °F] are shown in Table 3.

The potential-pH diagrams were calculated next using the adjusted solutions as the chemical environment (SCW, 0.19 M NaCl + 1.14 M  $\text{NaHCO}_3$ , 1.14 M  $\text{NaHCO}_3$ , and 0.19 M NaCl) and the Alloy 22 approximation as the surface material. Figures 1, 3, 5, and 7 show the calculated potential-pH diagrams for Alloy 22 in the four different solutions analyzed in this study. The diagrams shown represent the chromium and nickel systems of Alloy 22 in the different environments.

The Alloy 22 specimens evaluated by Chiang, et al.<sup>4</sup> were held potentiostatically at 100 and 400 mV versus a saturated calomel electrode (SCE). The calculated potential-pH diagrams present the potential results with respect to the standard hydrogen electrode (SHE). In order to

Ion	K <sup>+</sup>	Na <sup>+</sup>	Mg <sup>2+</sup>	Ca <sup>2+</sup>	F <sup>-</sup>	Cl <sup>-</sup>	NO <sub>3</sub> <sup>-</sup>	SO <sub>4</sub> <sup>2-</sup>	HCO <sub>3</sub> <sup>-</sup>
<b>M</b>	0.087	1.78	<4.1 × 10 <sup>-5</sup>	<2.5 × 10 <sup>-5</sup>	0.074	0.189	0.103	0.174	1.148

Environment	Cl <sup>-</sup>	NO <sub>3</sub> <sup>-</sup>	SO <sub>4</sub> <sup>2-</sup>	F <sup>-</sup>	HCO <sub>3</sub> <sup>-</sup>	CO <sub>3</sub> <sup>2-</sup>	Na <sup>+</sup>	K <sup>+</sup>	pH	
SCW	0.18	0.1	0.08	0.06	0.61	0.22	1.63	0.08	9*	25 °C [77 °F] 95 °C [203 °F]
	0.18	0.03	0.14	0.06	0.79	0.25	1.81	0.07	8.6†	
0.19 M NaCl+ 1.14 M NaHCO <sub>3</sub>	0.19	—	—	—	0.63	0.2	1.29	—	9*	25 °C [77 °F] 95 °C [203 °F]
	0.18	—	—	—	0.77	0.25	1.48	—	8.6†	
1.14 M NaHCO <sub>3</sub>	—	—	—	—	0.65	0.2	1.11	—	9*	25 °C [77 °F] 95 °C [203 °F]
	—	—	—	—	0.78	0.25	1.3	—	8.6†	
0.19 M NaCl	0.19	—	—	—	—	—	0.19	—	7	25 °C [77 °F] 95 °C [203 °F]
	0.18	—	—	—	—	—	0.18	—	6.2†	

\*pH adjustment to 9 at 25 °C [77 °F] for carbonate containing solutions with sodium hydroxide as titrant  
†calculated natural pH at 95 °C [203 °F]

compare the potential-pH diagrams to the experimental results, the experimental potentials were converted to the SHE scale, with the expression<sup>19</sup>

$$E_{SHE} = E_{SCE} + 0.2412 - 6.61 \times 10^{-4}(T - 25) - 1.75 \times 10^{-6}(T - 25)^2 - 9.0 \times 10^{-10}(T - 25)^3 \quad (1)$$

where  $T$  is the test temperature in centigrade units. At 95 °C [203 °F], the SCE potential values of 100 and 400 mV<sub>SCE</sub> were calculated to be 295 and 595 mV<sub>SHE</sub>, respectively.

## RESULTS

### Thermodynamic Analysis

The four solution compositions examined in this study were previously evaluated in the experiments by Chiang, et al.<sup>4</sup> to characterize the passive films on Alloy 22. In the study by Chiang, et al., the Alloy 22 samples were removed from the simulated solutions and examined with XPS. In this paper, these experimental results are compared to the calculated potential-pH diagrams to evaluate the potential existence of a chromium-rich oxide film in these solutions.

#### *Simulated Concentrated Water*

Simulated concentrated water was one of the environments examined by Chiang, et al.<sup>4</sup>, where a chromium oxide layer was not observed. Figure 1 shows the potential-pH diagrams for Alloy 22 in SCW for the (a) chromium species and (b) nickel species. The results from the thermodynamic calculations show that the natural pH was calculated to be 8.6 at 95 °C [203 °F]. At this pH and both potentials of 295 and 595 mV<sub>SHE</sub>, the chromium in the SCW would thermodynamically form solid Na<sub>2</sub>CrO<sub>4</sub>·10H<sub>2</sub>O while the nickel would form NiCr<sub>2</sub>O<sub>4</sub>. Both of these oxides are chromium-rich. Comparing this to the experimental results, Figure 2 shows the XPS profiles by Chiang, et al. for SCW.<sup>4</sup> The film formed at 295 mV<sub>SHE</sub> is thinner than the oxide formed at 595 mV<sub>SHE</sub>. In addition, there is a silica film observed on the surface of the passive film at both potentials. A chromium-rich oxide cannot be identified at either of the two potentials which is different compared to the thermodynamic results. However, nickel oxide is observed at both potentials. The nickel oxide appears more abundant at 595 mV<sub>SHE</sub>.

#### *HCO<sub>3</sub><sup>-</sup> as in Simulated Concentrated Water*

As discussed in the introduction, bicarbonate solutions were examined by Chiang, et al.<sup>4</sup> because of their connection to stress corrosion cracking. Figure 3 shows the potential-pH diagrams for Alloy 22 in the 1.14 M NaHCO<sub>3</sub> for (a) chromium species and (b) nickel species. The results indicate that the natural pH should be 8.6 at 95 °C [203 °F], which is the same as the SCW solution. The thermodynamic calculations indicate thermodynamically stable CrO<sub>4</sub><sup>2-</sup>. At the natural pH and the polarization potentials in these tests, the CrO<sub>4</sub><sup>2-</sup> would be expected to be a stable aqueous phase. The nickel potential-pH diagram on Alloy 22 was similar to that of the SCW potential-pH results with a thermodynamically stable phase of NiCr<sub>2</sub>O<sub>4</sub>. The experimental results by Chiang, et al.<sup>4</sup> are shown in Figure 4. Similar to the SCW results, the films on the surface of Alloy 22 are thicker at 595 mV<sub>SHE</sub> than 295 mV<sub>SHE</sub>. A chromium oxide is observable on the sample held at 295 mV<sub>SHE</sub>, but not on the sample at 595 mV<sub>SHE</sub>. The Alloy 22 sample that was held at 595 mV<sub>SHE</sub> seems to be composed of a nickel oxide layer under the silica contamination layer.

#### *Cl<sup>-</sup> and HCO<sub>3</sub><sup>-</sup> as in Simulated Concentrated Water*

Another mildly alkaline solution where the chromium oxide was not observed<sup>4</sup> was 0.19 M NaCl + 1.14 M NaHCO<sub>3</sub>. Figure 5 shows the potential-pH diagrams for Alloy 22 in 0.19 M NaCl + 1.14 M NaHCO<sub>3</sub> solution for the (a) chromium species and (b) nickel species. The calculated results indicate that the natural pH should again be 8.6 at 95 °C [203 °F], which is the same as the previous two solutions discussed. The results are the same as the 1.14 M NaHCO<sub>3</sub>. The potential-pH calculations indicate that the thermodynamically stable chromium phase at 295 and 595 mV<sub>SHE</sub> was CrO<sub>4</sub><sup>2-</sup> in solution, while the nickel phase would be NiCr<sub>2</sub>O<sub>4</sub>. The XPS experimental results of Alloy 22 in 0.19 M NaCl + 1.14 M NaHCO<sub>3</sub> solution<sup>4</sup> are shown in Figure 6. The XPS results from the sample held at 295 mV<sub>SHE</sub> indicate a porous silica film on the outer layer with some type of hydroxide layer underneath. Below this hydroxide layer was a distinct chromium-rich oxide which was similar to the results at 295 mV<sub>SHE</sub> in the 1.14 M NaHCO<sub>3</sub> solution. The sample held at 595 mV<sub>SHE</sub> in the 0.19 M NaCl + 1.14 M NaHCO<sub>3</sub> solution did not indicate the presence of a chromium oxide. Instead, a nickel oxide was found below a porous silica and hydroxide layer. While the thermodynamic calculations suggest the presence of a Ni-Cr oxide at 595 mV<sub>SHE</sub>, none was observed.

#### *Cl<sup>-</sup> as in Simulated Concentrated Water*

In addition to the mild alkaline environments study by Chiang et al.,<sup>4</sup> a few neutral solutions were also examined experimentally, including a 0.19 M NaCl solution. Chloride has been suggested to be a chemical species known to break down the oxide film.<sup>20</sup> Therefore, this analysis is included in the current study. The results of the potential-pH diagrams are not very different from the other solutions, and these results are shown in Figure 7. The HCrO<sub>4</sub><sup>-</sup> in solution is a thermodynamically stable phase at 595 mV<sub>SHE</sub>. The result for nickel in the Alloy 22 is similar to the other solutions, which indicates that the thermodynamically stable nickel phase is NiCr<sub>2</sub>O<sub>4</sub>. The surface film analysis for Alloy 22 in the 0.19 M NaCl solution at 595 mV<sub>SHE</sub> is shown in Figure 8. There is a substantial chromium-rich oxide found on the surface of Alloy 22 in this environment, which correlates well with the thermodynamic data.

## DISCUSSION

The corrosion performance of the waste package outer barrier is considered to be dependent upon the integrity of a thin and compact passive film on the Alloy 22 surface. The low general corrosion rates and resistance to localized corrosion over the extended performance periods are dependent upon the long-term stability and integrity of the passive film. Chromium oxide passive films have been difficult to observe in some solutions where their presence is expected. Because low corrosion rates were measured in these environments, it is believed that the chromium-rich inner layer oxide was present, but was undetected. However, the presence of silica and/or carbon film on the surface of the Alloy 22 may also lead to decreased corrosion rates, so additional data are necessary to determine the properties of the passive film in these various solutions.

Various simulated environments were experimentally evaluated in the study by Chiang, et al.<sup>4</sup> The passive films were characterized using XPS. The thermodynamic study reported in this paper examined the same solutions and compared the results with the XPS analyses. The results of the experimental and thermodynamic studies at 95 °C [203 °F] are summarized in Table 4.

<b>Solution</b>	<b>Potential (mV<sub>SHE</sub>)</b>	<b>Chromium Oxide Observed (Exp.)</b>	<b>Nickel Thermodynamically Preferred State</b>	<b>Chromium Thermodynamically Preferred State</b>
Simulated concentrated water	295	No	NiCr <sub>2</sub> O <sub>4</sub>	Na <sub>2</sub> CrO <sub>4</sub> ·10H <sub>2</sub> O
Simulated concentrated water	595	No	NiCr <sub>2</sub> O <sub>4</sub>	Na <sub>2</sub> CrO <sub>4</sub> ·10H <sub>2</sub> O
1.14 M NaHCO <sub>3</sub>	295	Yes	NiCr <sub>2</sub> O <sub>4</sub>	CrO <sub>4</sub> <sup>2-</sup>
1.14 M NaHCO <sub>3</sub>	595	No	NiCr <sub>2</sub> O <sub>4</sub>	CrO <sub>4</sub> <sup>2-</sup>
0.19 M NaCl + 1.14 M NaHCO <sub>3</sub>	295	Yes	NiCr <sub>2</sub> O <sub>4</sub>	CrO <sub>4</sub> <sup>2-</sup>
0.19 M NaCl + 1.14 M NaHCO <sub>3</sub>	595	No	NiCr <sub>2</sub> O <sub>4</sub>	CrO <sub>4</sub> <sup>2-</sup>
0.19 M NaCl	595	Yes	NiCr <sub>2</sub> O <sub>4</sub>	HCrO <sub>4</sub> <sup>-</sup>

As can be observed from the data presented in Table 4, the thermodynamic calculations indicate that a chromium-rich oxide should be observed in the environments considered in this study. Chromium in the various environments has several thermodynamically stable states, while nickel was only stable as NiCr<sub>2</sub>O<sub>4</sub> for each of the environments examined.

A chromium-rich oxide is experimentally observed in the pH 9 solutions at 295 mV<sub>SHE</sub>, except for the case of the SCW solution. Examining the various potential-pH diagrams for the solution/pH combination where the chromium-rich oxide was observed, the thermodynamically calculated phases for chromium are only tens of mVs from the stable Cr<sub>2</sub>O<sub>3</sub> phase region. Similarly, a chromium-rich oxide was observed in the NaCl only solution at 595 mV<sub>SHE</sub>, which is again only tens of mVs away from the Cr<sub>2</sub>O<sub>3</sub> phase region. The proximity to the thermodynamically stable Cr<sub>2</sub>O<sub>3</sub> phase region may relate to the observable chromium-rich oxide in some of these solutions. However, the location on the potential-pH diagram for simulated concentrated water at 295 mV<sub>SHE</sub> is also only tens of mVs from the Cr<sub>2</sub>O<sub>3</sub> phase region and a chromium-rich oxide was not observed in the experimental XPS analysis for this solution.

After polarizing to 595 mV<sub>SHE</sub>, chromium oxide disappeared from the 0.19 M NaCl + 1.14 M NaHCO<sub>3</sub> and 1.14 M NaHCO<sub>3</sub> solutions. The thermodynamically stable phases present at 595 mV<sub>SHE</sub> are not different from those calculated at 295 mV<sub>SHE</sub> for the respective solutions. At 595 mV<sub>SHE</sub>, the potential-pH location is farther from the Cr<sub>2</sub>O<sub>3</sub> phase region than at 295 mV<sub>SHE</sub>,

but  $\text{NiCr}_2\text{O}_4$  is still calculated to be stable. One of the main differences between the two potentials is that the overall passive film thickness is much larger at  $595 \text{ mV}_{\text{SHE}}$  than  $295 \text{ mV}_{\text{SHE}}$ . As mentioned previously, the passive film is considered to be composed of an inner chromium-rich film and an outer nickel/iron oxi-hydroxide film. In these higher potentials, the outer film may become thicker and the addition of a silica/carbon contamination layer may make it difficult to measure the chromium oxide film with XPS. The results by Chiang, et al. indicated that at higher potentials the films tend to be thicker.<sup>4</sup> In addition, Jabs, et al.<sup>21</sup> indicated that the concentration of chromium(VI) ions will increase as the potential is raised, and these chromium(VI) ions can easily become soluble in the alkaline pH environments.

While the chromium oxide disappeared at  $595 \text{ mV}_{\text{SHE}}$ , the nickel oxide presence on Alloy 22 increased in the mildly alkaline solutions. The nickel potential-pH diagrams indicate that as the potential is increased, the nickel phase is approaching the  $\text{Ni}_3\text{O}_4$  region. In addition to the thermodynamic change from a chromium-nickel oxide to the nickel oxide, the solubility of nickel hydroxide in alkaline solutions is low. Both the solubility and thermodynamic features are possible reasons why a nickel oxide is more abundant at  $595 \text{ mV}_{\text{SHE}}$ .

Alloy 22 has been experimentally evaluated in some mildly alkaline environments where a chromium-oxide was both observed and not observed. It has been assumed that the chromium-oxide is present because of low corrosion rates. However, silica/carbon films observed on these samples dilute this argument because of their ability to reduce the corrosion rate. The thermodynamic calculations suggest that a  $\text{NiCr}_2\text{O}_4$  is stable in all the environments examined. Therefore, the analyses suggest that because nothing is thermodynamically different between the particular potential/solution environments where a chromium-rich oxide is not observed and the potential/solution environments where chromium-rich oxide is observed, the chromium-rich oxide is expected to be present. Even if local environments different than the bulk conditions develop, it would not be expected to change the thermodynamic conditions significantly. The results presented in this study suggest the existence of a nickel-chromium oxide film reducing the corrosion rates that is not detectable by the XPS system. The inability to observe the nickel-chromium oxide film was possibly due to the thinness of the film in conjunction with thicker outer layers masking the inner film.

## CONCLUSION

To investigate the formation of a chromium-rich passive film on the surface of Alloy 22 in mildly alkaline environments, Corrosion Analyzer software was used to construct potential-pH diagrams. The potential-pH diagrams were compared to experimental tests by Chiang, et al.,<sup>4</sup> where the chromium-rich oxide film was not observed.

The amount of nickel oxide in the passive film increased experimentally as the electrochemical potential was raised. This was attributed to the low solubility of nickel in alkaline environments and the thermodynamic data that suggested that increasing the potential causes an evolution toward a pure nickel oxide versus a mixed nickel chromium oxide.

The chromium-rich oxide was observed in the alkaline pH solutions at  $295 \text{ mV}_{\text{SHE}}$  but not at  $595 \text{ mV}_{\text{SHE}}$ , except for the SCW solution where no chromium-rich oxide was observed at either potential. The change in the presence of chromium-rich oxides at the two potentials in the  $0.19 \text{ M NaCl} + 1.14 \text{ M NaHCO}_3$  and  $1.14 \text{ M NaHCO}_3$  solutions is believed to be due to higher solubility of Cr(VI) at  $595 \text{ mV}_{\text{SHE}}$  and a thicker outer film. It is still unclear as to why the



chromium-rich oxide was not observed in the SCW solution at 295 mV<sub>SHE</sub>, because the thermodynamic data and other research conducted in alkaline environments suggest the existence of a NiCr<sub>2</sub>O<sub>4</sub> film in all of the solutions and potentials examined.

### **DISCLAIMER**

This paper describes work performed by the Center for Nuclear Waste Regulatory Analyses (CNWRA) for the U.S. Nuclear Regulatory Commission (NRC) under contract number NRC-02-02-012. The activities reported here were performed on behalf of the NRC Office of Nuclear Material Safety and Safeguards, Division of High-Level Waste Repository Safety. This paper is an independent product of CNWRA and does not necessarily reflect the view or regulatory position of NRC. The NRC staff views expressed herein are preliminary and do not constitute a final judgment or determination of the matters addressed or of the acceptability of a license application for a potential geologic repository at Yucca Mountain.

### **ACKNOWLEDGMENTS**

The authors gratefully acknowledge the reviews of Drs. O. Pensado and S. Mohanty, the editorial review of L. Mulverhill, and the assistance of B. Street in the preparation of this manuscript. We would like to thank Dr. R. Pabalan for technical discussions in the development of this paper.

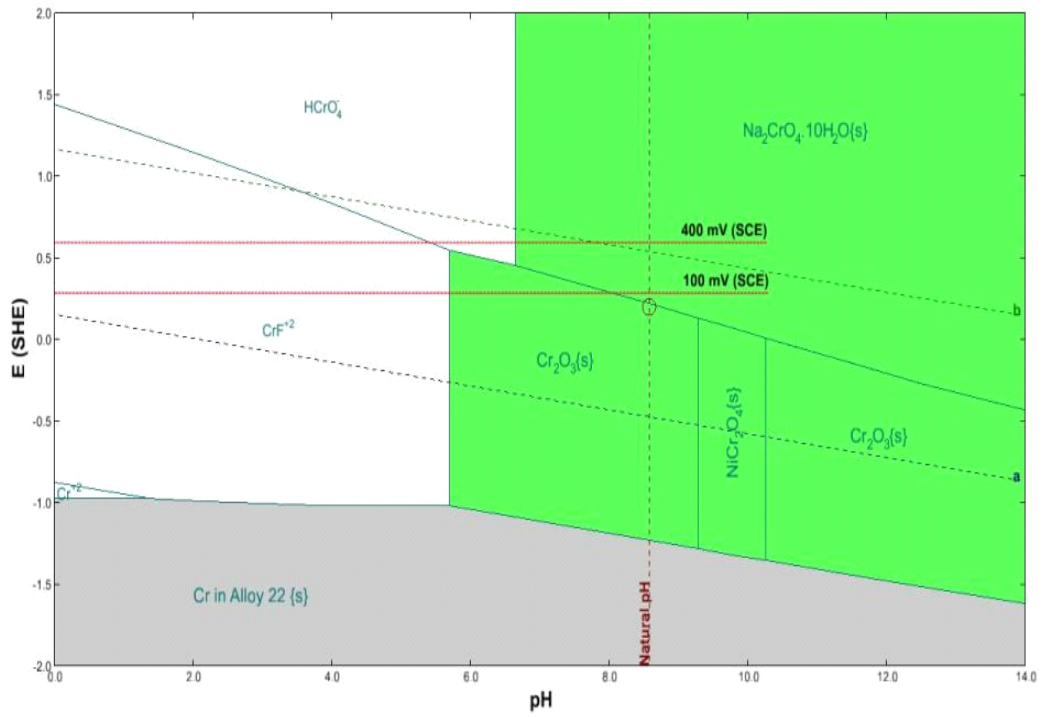
### **REFERENCES**

1. Bechtel SAIC Company, LLC, "Technical Basis Document No. 6: Waste Package and Drip Shield Corrosion," Rev. 01, Las Vegas, Nevada: Bechtel SAIC Company, LLC, 2003.
2. D.S. Dunn, O. Pensado, Y.-M. Pan, R.T. Pabalan, L. Yang, X. He, and K.T. Chiang, "Passive and Localized Corrosion of Alloy 22—Modeling and Experiments," CNWRA 2005-02, Rev. 1, San Antonio, Texas: Center for Nuclear Waste Regulatory Analyses, 2005.
3. M.F. Montemor, M.G.S. Ferreira, N.E. Hakiki, and M. Da Cunha Belo, "Chemical composition and electronic structure of the oxide films formed on 316L stainless steel and nickel based alloys in high temperature aqueous environments," Corrosion Science, Vol. 42, pp. 1635–1650, 2000.
4. K.T. Chiang, D.S. Dunn, Y.-M. Pan, O. Pensado, and P.K. Shukla, "Stress Corrosion Cracking of Waste Package Material—Modeling and Experiments," CNWRA 2007-001, San Antonio, Texas: Center for Nuclear Waste Regulatory Analyses, 2007.
5. C.A. Orme, "The Passive Film on Alloy 22," UCRL-TR-215277, Livermore, California: Lawrence Livermore National Laboratory, 2005.
6. Bechtel SAIC Company, LLC, "General Corrosion and Localized Corrosion of Waste Package Outer Barrier," ANL-EBS-MD-000003, Rev. 02, Las Vegas, Nevada: Bechtel SAIC Company, LLC, 2004.

7. J.R. Hayes, J.J. Gray, A.W. Szmodis, and C.A. Orme, "Influence of chromium and molybdenum on the corrosion of nickel-based alloys," *Corrosion*, Vol. 62, pp. 491–500, 2006.
8. S.T. Amaral and I.L. Muller, "Effect of silicate on passive films anodically formed on iron in alkaline solution as studied by electrochemical impedance spectroscopy," *Corrosion*, Vol. 55, pp. 17–23, 1999.
9. A.A. Hermas, K. Ogura, S. Takagi, and T. Adachi, "Effects of alloying additions on corrosion and passivation behaviors of type 304 stainless steel," *Corrosion*, Vol. 51, pp. 3–10, 1995.
10. M. Navas, D. Gómez-Briceño, M. García-Mazario, and A.R. McIlree, "Effect of silicon compounds on stress corrosion cracking of alloy 600 in caustic solutions," *Corrosion*, Vol. 55, pp. 674–685, 1999.
11. R.W. Staehle and J.A. Gorman, "Quantitative assessment of submodes of stress corrosion cracking on the secondary side of steam generator tubing in pressurized water reactors: part 2," *Corrosion*, Vol. 60, pp. 5–63, 2004.
12. W. Ensinger, O. Lensch, T. Matsutani, and M. Kiuchi, "Corrosion performance of thin amorphous carbon films on aluminum formed by ion beam-based coating techniques," *Surface & Coatings Technology*, Vol. 196, pp. 231–235, 2005.
13. J. Von Ringleben, Ch. Sundermann, T. Matsutani, M. Kiuchi, and E. Ensinger, "Sealing performance of thin amorphous carbon films formed by ion beam assisted deposition at low temperature for protection of aluminum against aggressive media: the influence of the ion energy," *Thin Solid Films*, Vol. 482, pp. 115–119, 2005.
14. J.H. Sui and W. Cai, "Effect of bias voltage on the structure and the electrochemical corrosion behavior of hydrogenated amorphous carbon (a-C:H) films on NiTi alloys," *Surface & Coatings Technology*, Vol. 201, pp. 6906–6909, 2007.
15. A. Anderko and M.M. Lencka "Computation of electrical conductivity of multicomponent aqueous systems in wide concentration and temperature ranges," *Industrial and Engineering Chemistry Research*, Vol. 36, pp. 1932–1943, 1997.
16. A. Anderko and M. M. Lencka,, "Modeling transport properties of electrolyte solutions in wide concentration and temperature ranges," *Power Plant Chemistry*, Vol. 2, No. 9, pp. 523–528, 2000.
17. A. Anderko, S.J. Sanders, and R.D. Young, "Real-solution stability diagrams: a thermodynamic tool for corrosion modeling," *Corrosion*, Vol. 53, pp. 43–53, 1997.
18. Bechtel SAIC Company, LLC, "Technical Basis Document No. 5: In-Drift Chemical Environment," Rev 01, Las Vegas, Nevada: Bechtel SAIC Company, LLC, 2003.

19. L. Meites, "Handbook of Analytical Chemistry," New York City, New York: McGraw-Hill Book Company, 1963.
20. D.D. MacDonald, "The point defect model for the passive state," *Journal of Electrochemical Society*, Vol. 139, pp. 3434–3449, 1992.
21. T. Jabs, P. Borthen, and H.-H. Strehblow, "X-ray photoelectron spectroscopic examinations of electrochemically formed passive layers on Ni-Cr alloys," *Journal of the Electrochemical Society*, Vol. 144, pp. 1231–1243, 1997.

(a) Cr



(b) Ni

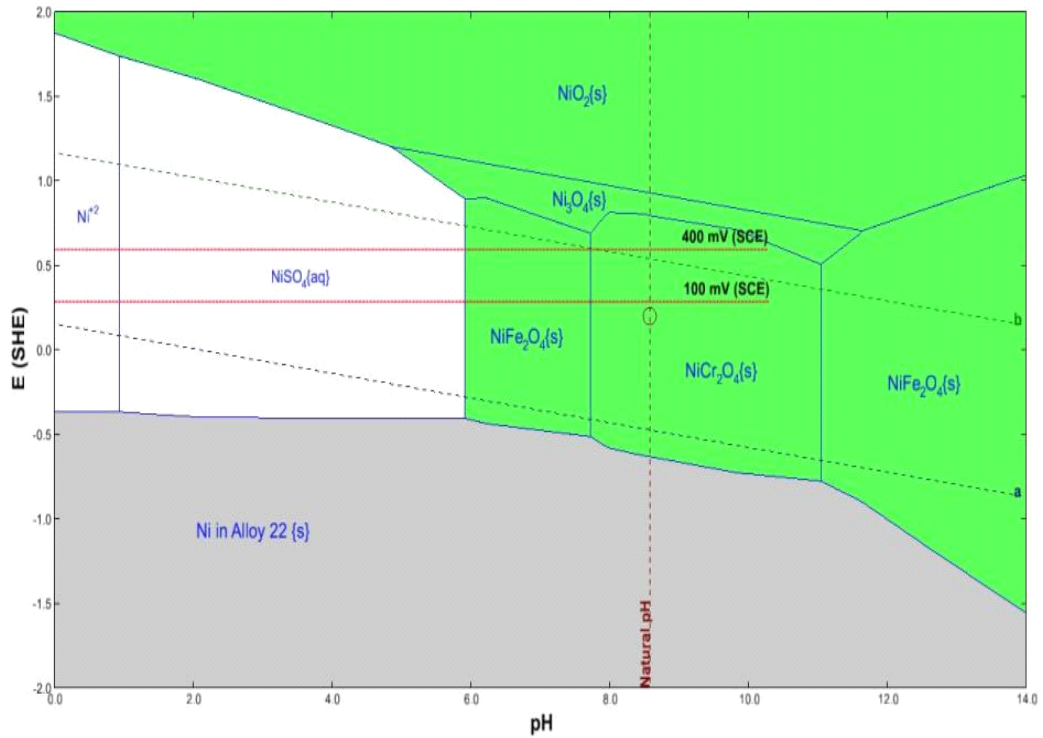


Figure 1. Potential-pH diagrams for Alloy 22 in simulated concentrated water at 95 °C [203 °F] for (a) chromium species and (b) nickel species.

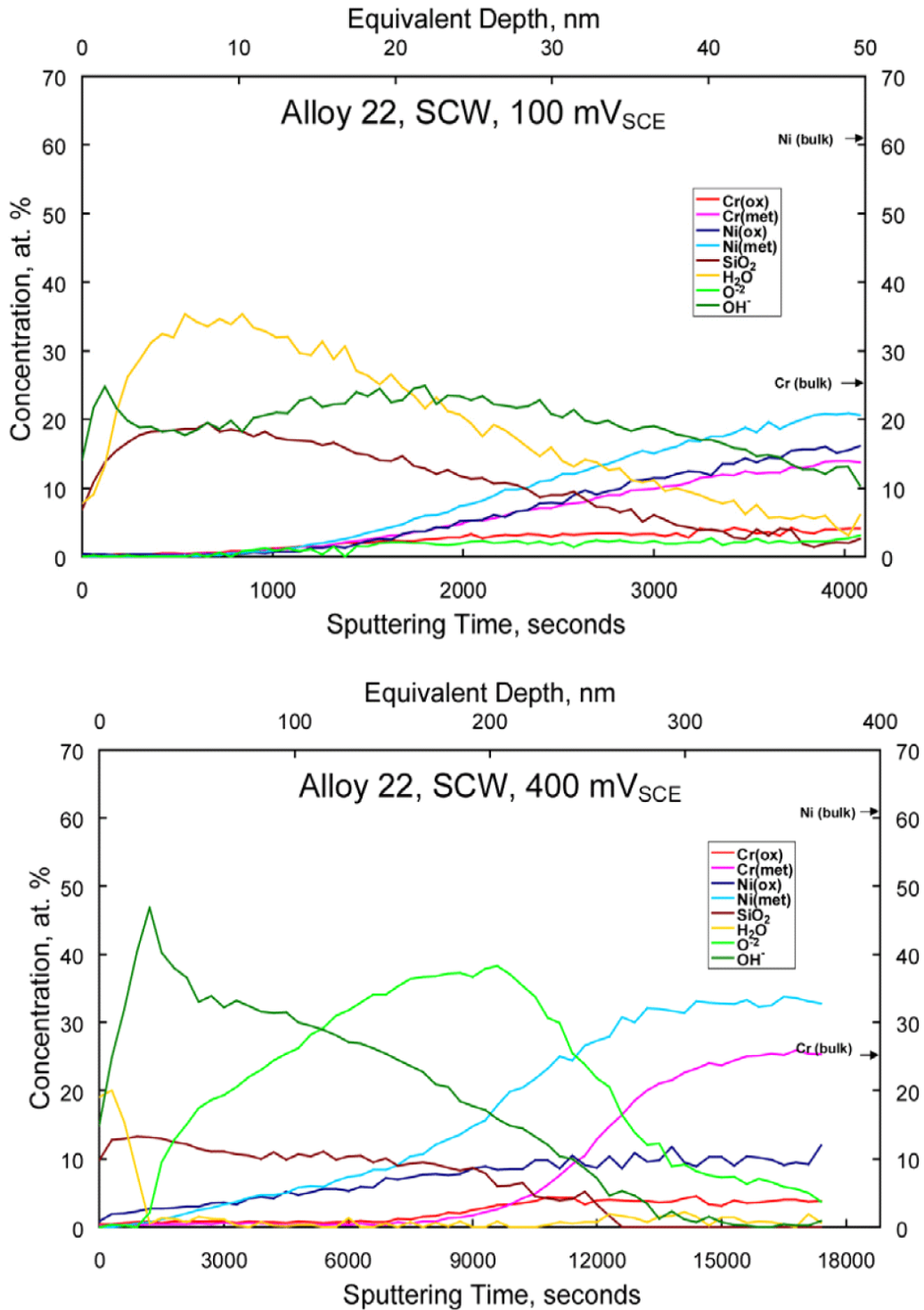
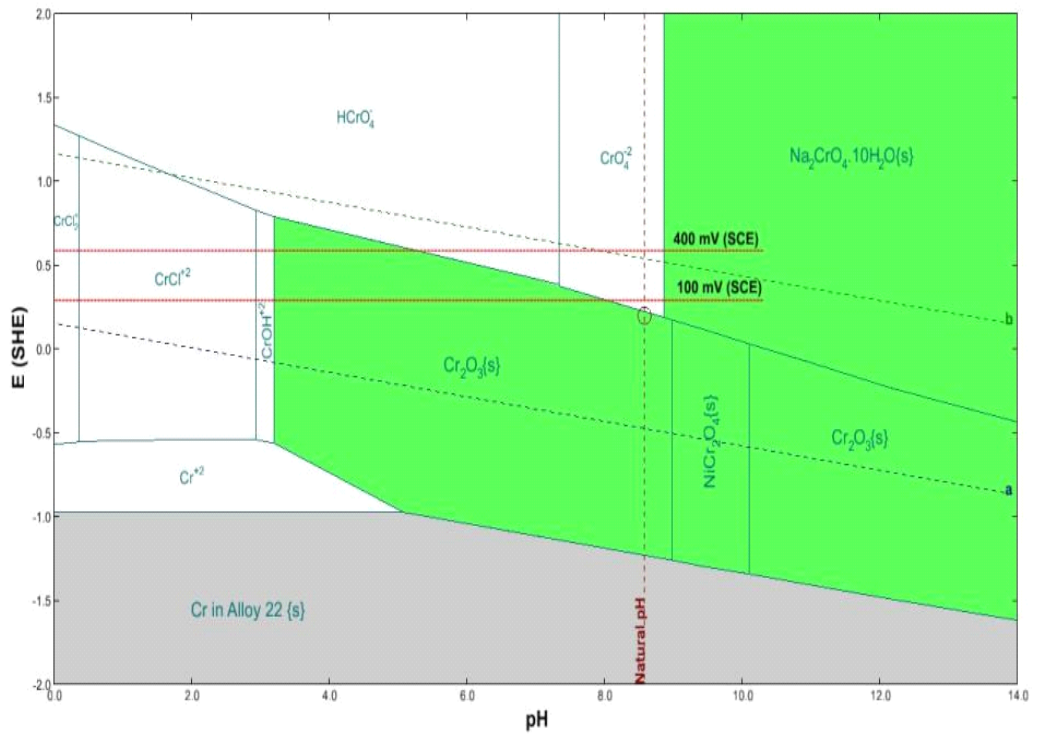


Figure 2. X-ray photoelectron spectroscopy depth profiles of Alloy 22 electrochemically treated in deaerated simulated concentrated water at 95 °C [203 °F] for an applied potential of 295 mV<sub>SHE</sub> (top) and 595 mV<sub>SHE</sub> (bottom) (Chiang, et al.<sup>4</sup>).

(a) Cr



(b) Ni

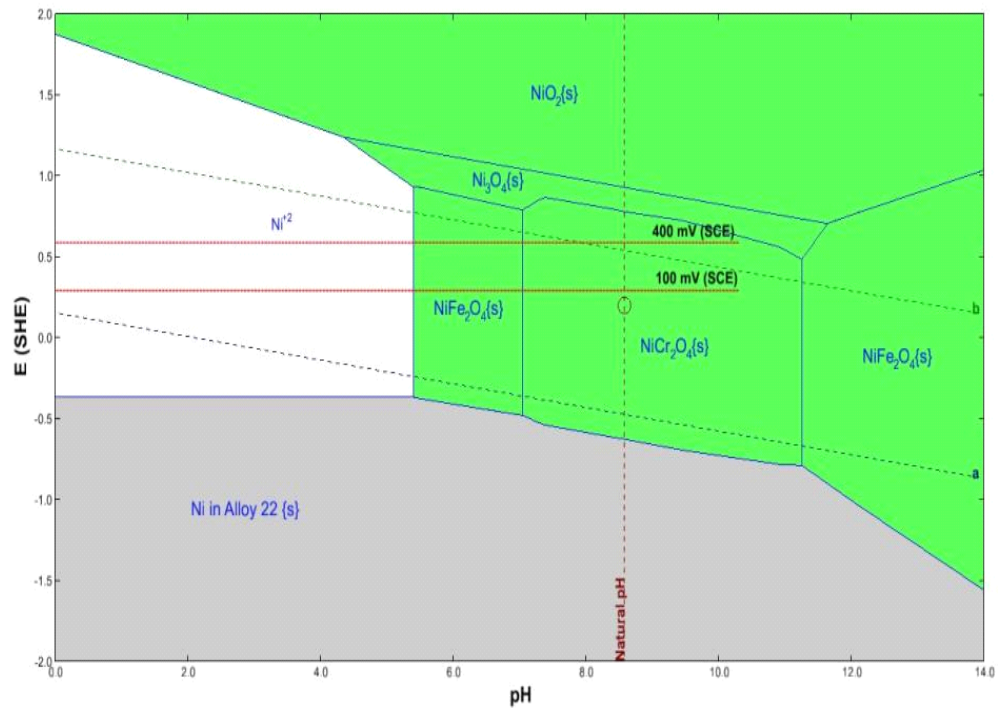


Figure 3. Calculated potential-pH diagram set for Alloy 22 in 1.14 M  $\text{NaHCO}_3$  at 95 °C [203 °F] for (a) chromium species and (b) nickel species.

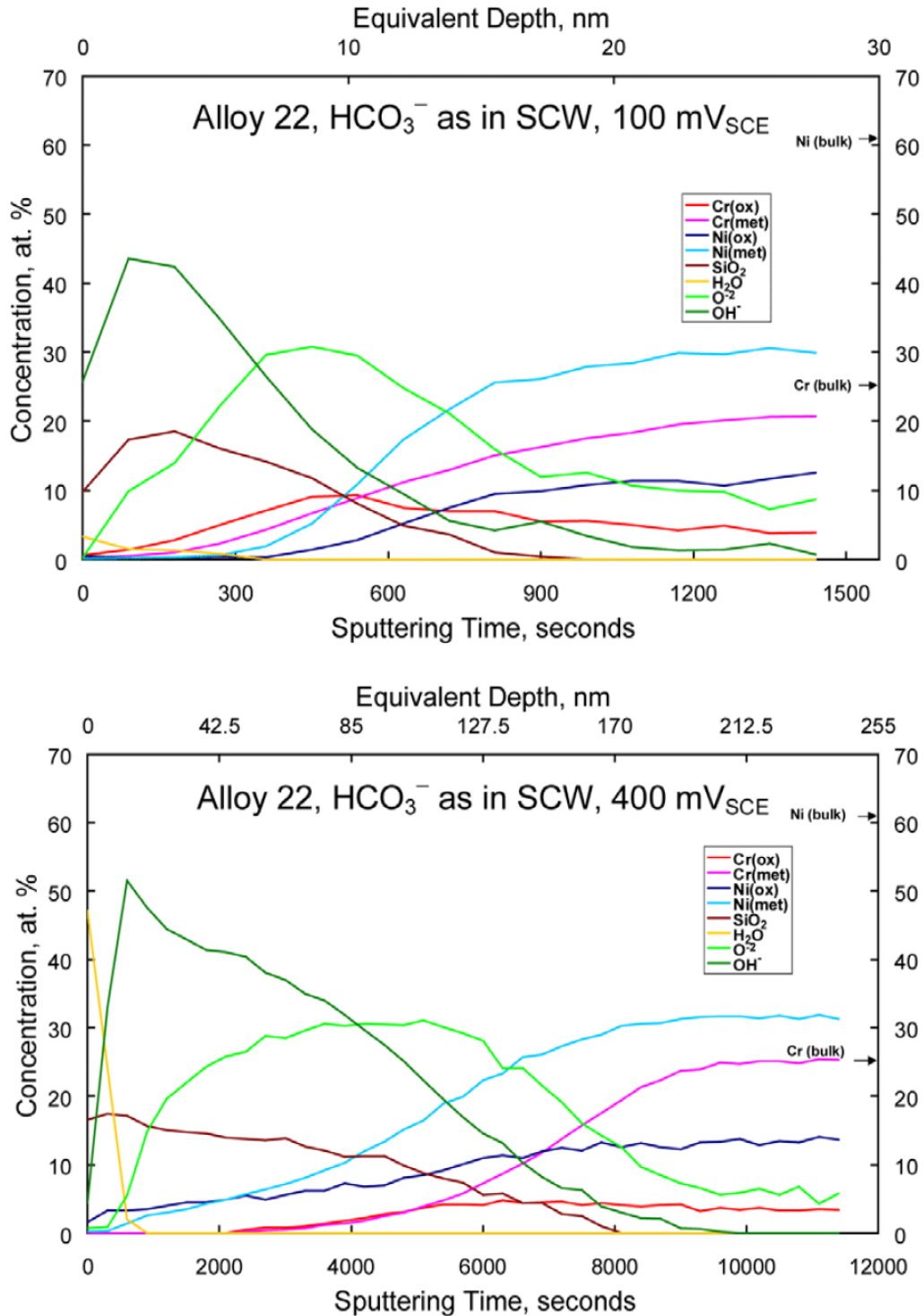
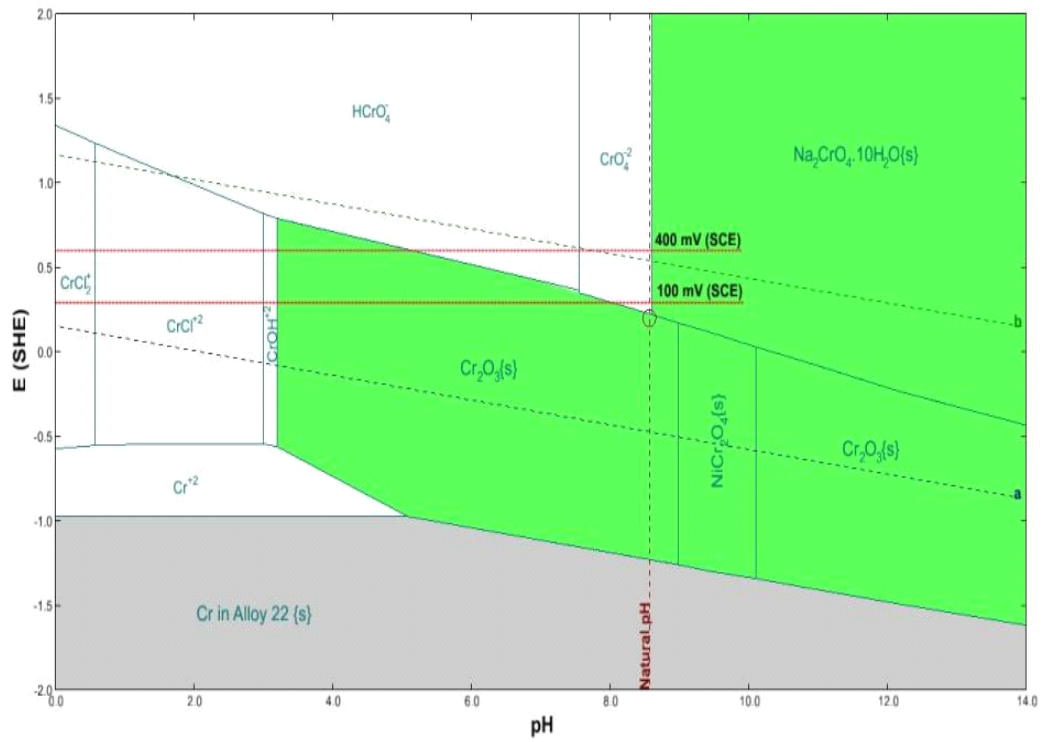


Figure 4. X-ray photoelectron spectroscopy depth profiles of Alloy 22 electrochemically treated in deaerated 1.14 M  $\text{NaHCO}_3$  {same  $[\text{HCO}_3^-]$  as in simulated concentrated water} at  $95 \text{ }^\circ\text{C}$  [ $203 \text{ }^\circ\text{F}$ ] for an applied potential of  $295 \text{ mV}_{\text{SHE}}$  (top) and  $595 \text{ mV}_{\text{SHE}}$  (bottom) (Chiang, et al.<sup>4</sup>).

(a) Cr



(b) Ni

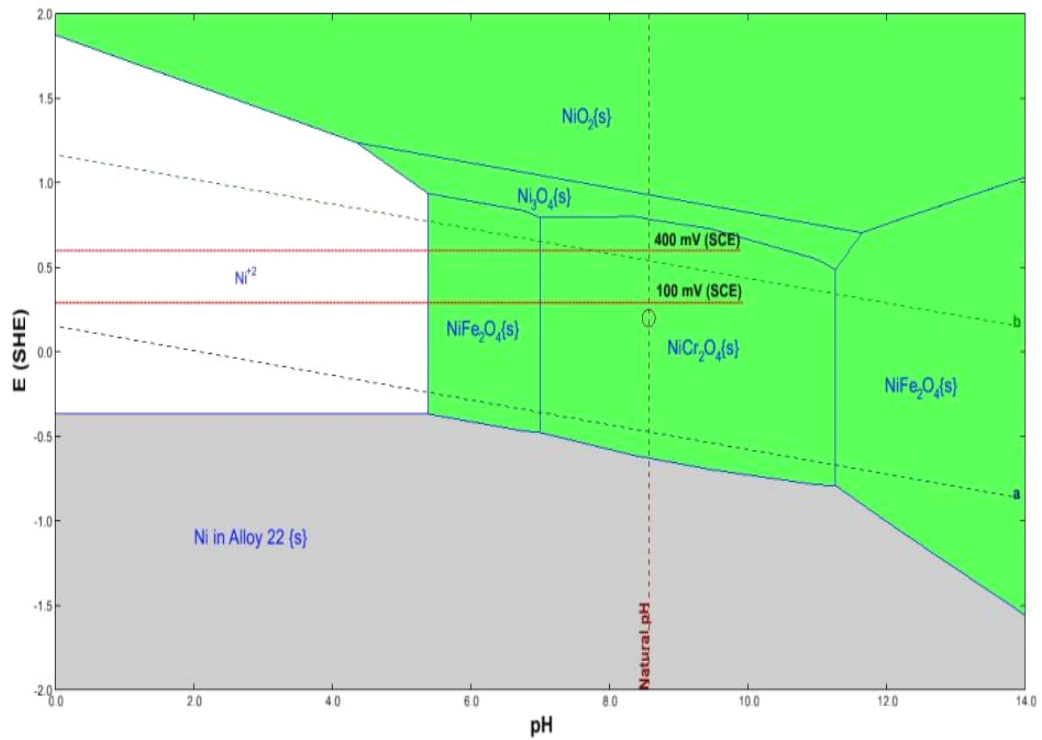


Figure 5. Calculated potential-pH diagram set for Alloy 22 in 0.19 M NaCl + 1.14 M NaHCO<sub>3</sub> at 95 °C [203 °F] for (a) chromium species and (b) nickel species.



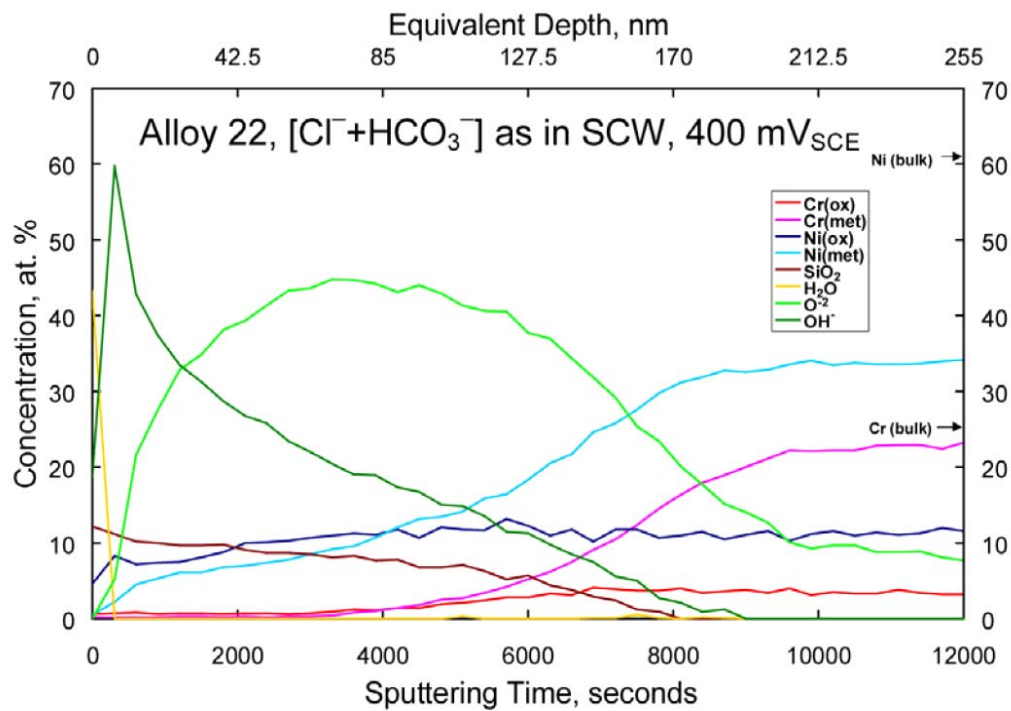
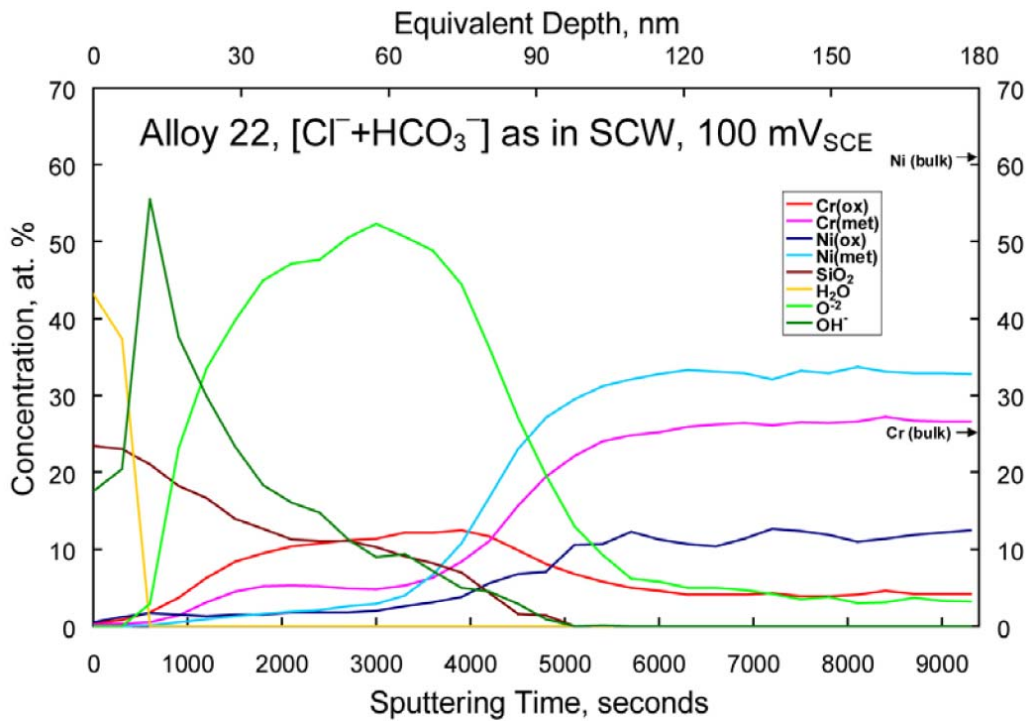
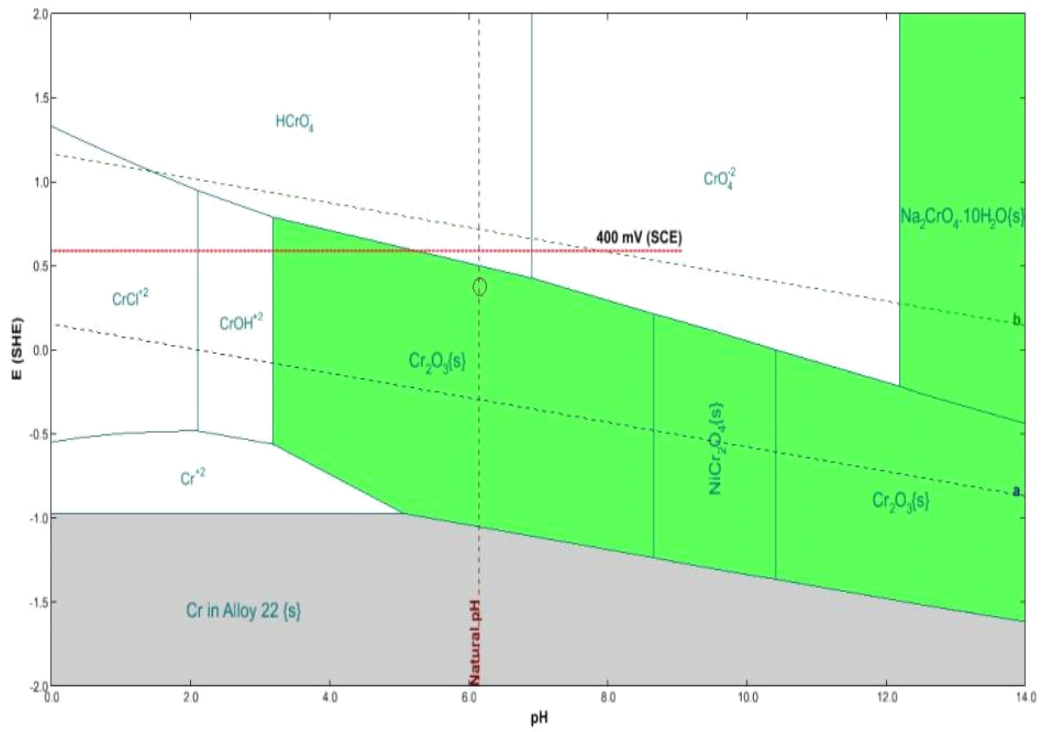


Figure 6. X-ray photoelectron spectroscopy depth profiles of Alloy 22 electrochemically treated in deaerated in 0.19 M NaCl + 1.14 M NaHCO<sub>3</sub> {same [Cl<sup>-</sup>] and [HCO<sub>3</sub><sup>-</sup>] as in simulated concentrated water} at 95 °C [203 °F] for an applied potential of 295 mV<sub>SHE</sub> (top) and 595 mV<sub>SHE</sub> (bottom) (Chiang, et al.<sup>4</sup>).

(a) Cr



(b) Ni

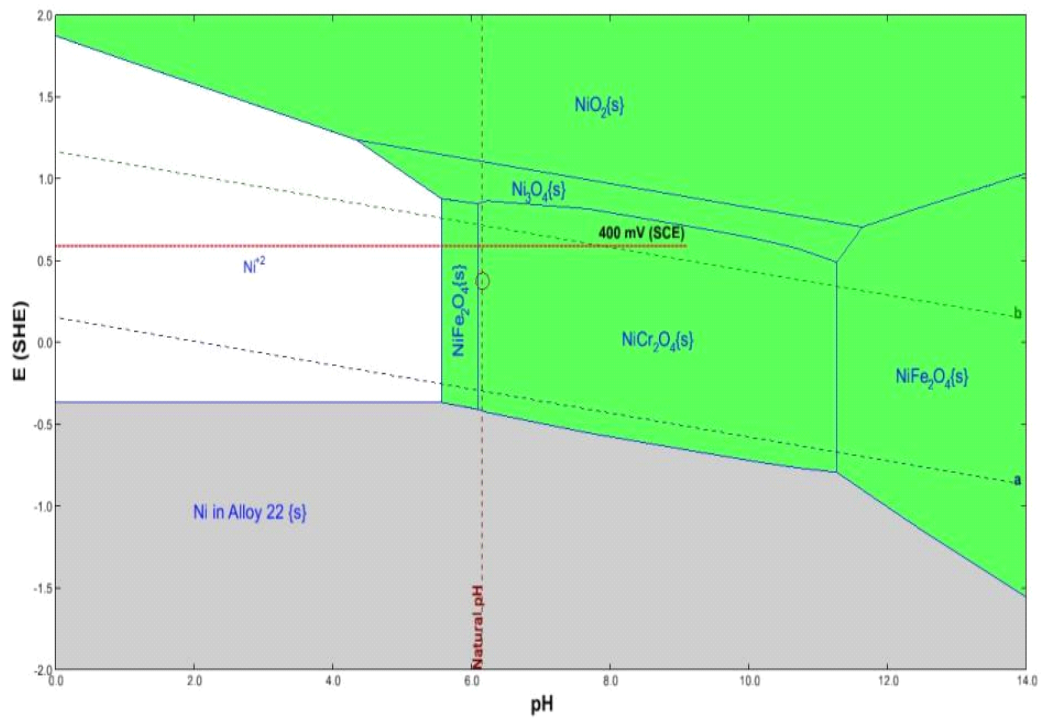


Figure 7. Calculated potential-pH diagram set for Alloy 22 in 0.19 M NaCl at 95 °C [203 °F] for (a) chromium species and (b) nickel species.

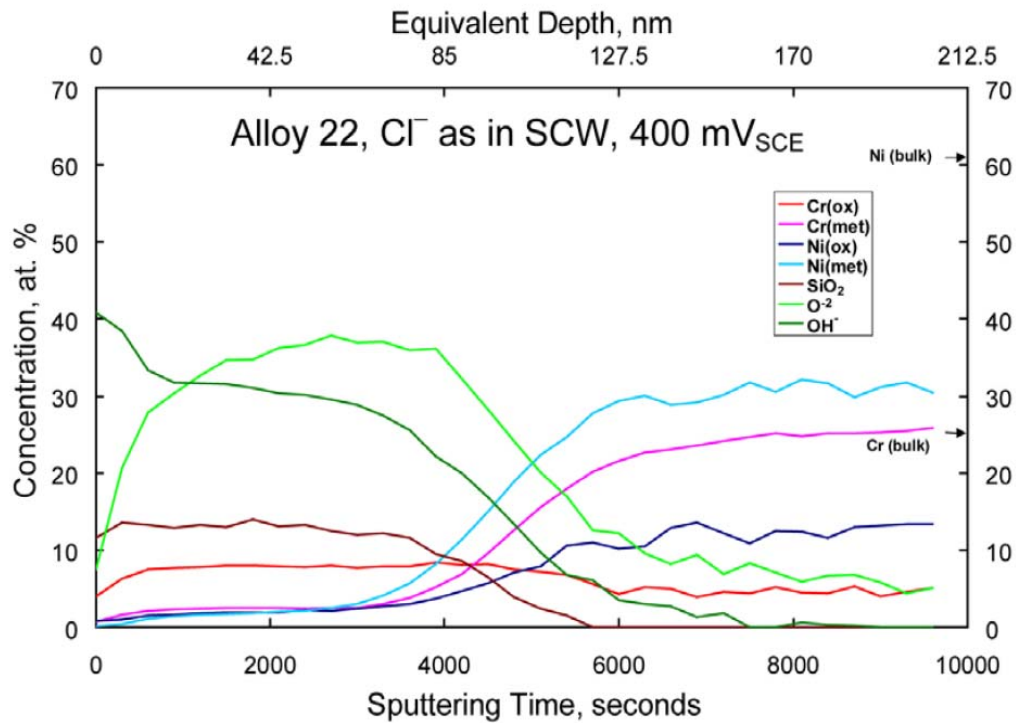


Figure 8. X-ray photoelectron spectroscopy depth profiles of Alloy 22 electrochemically treated in deaerated in 0.19 M NaCl {same [Cl<sup>-</sup>] as in simulated concentrated water} at 95 °C [203 °F] for an applied potential of 595 mV<sub>SHE</sub> (Chiang, et al.<sup>4</sup>).